Research Article | Vol. 32, No. 13 / 17 Jun 2024 / Optics Express 23702
Optics EXPRESS

Optical integrated reconfigurable mode generator-multiplexer for radio-frequency orbital angular momentum

YUANHUA FENG,[1,†] SHECHENG GAO,[1,†] JIAJIE ZHANG,[1] AMIR ABBAS KASHI,[2] GIJS VAN ELZAKKER,[2] XUEBING ZHANG,[2,*] RUUD OLDENBEUVING,[2] AND TON KOONEN[3]

[1]*Department of Electronic Engineering, College of Information Science and Technology, Jinan University, Guangzhou 510630, China*
[2]*IMEC The Netherlands, HTC31 5656 AE, Eindhoven, Netherlands*
[3]*Eindhoven University of Technology, 5600 MB, Eindhoven, Netherlands*
[†]These authors contributed equally to this work.
[*]*Xuebing.Zhang@imec.nl*

Abstract: Radio-frequency orbital angular momentum (RF-OAM) mode multiplexing has received increasing attention in next-generation (6G) wireless communication as a new spatial multiplexing dimension to further extend data capacity. In particular, the circular antenna array (CAA) based RF-OAM generation using photonic methods is a promising approach due to its flexible reconfigurability, low propagation loss, high operating bandwidth, and high pattern quality. However, most current reports focus either on the bulk optics-based implementations or on band-limited delay line-based approaches. In this paper, we present a novel phased array-based integrated photonic RF-OAM generator-multiplexer for a four-antenna CAA system supporting three RF-OAM modes at 16 GHz for both fast mode switching and mode multiplexing. It consists of a specially designed interleaved optical filter and a four-element phased array based on cascaded phase shifters. By changing the pair of wavelengths used, the output RF-OAM modes can be quickly switched between fundamental mode and ±1 modes. A bandwidth of 1 GHz was experimentally demonstrated. Mode multiplexing can be achieved when all three wavelength pairs are loaded.

© 2024 Optica Publishing Group under the terms of the Optica Open Access Publishing Agreement

1. Introduction

As a new spatial multiplexing dimension, orbital angular momentum (OAM) can provide potentially huge wireless capacity by providing multiple spatial channels. OAM is associated with the helicoidal phase profile of an electromagnetic wave in a plane perpendicular to the propagation direction. Different OAM modes are orthogonal to each other, and each can carry large data streams. Therefore, OAM has been widely considered for high-capacity communications in optical and radio wireless systems [1,2]. OAM at radio frequency (RF-OAM) based on a circular antenna array (CAA) with specific phase differences induced between the antenna elements, is considered as a promising approach to further extend the RF wireless capacity as it can generate reconfigurable RF-OAM beams containing multiple modes carrying independent data streams at the same time [3–5]. In general, to generate RF-OAM modes, an accurate broadband phase shift among the modes is required, and the phase shifts induced by the phase shifter should be the same for the full range of frequencies in the data stream [6]. However, it is not easy to support wideband RF-OAM multiplexing (e.g., millimeter-wave signals) with electronics alone due to limited bandwidth, high losses, and low phase-shift resolution [7,8]. Photonic-assisted RF-OAM generation techniques utilizing optical true time delay (OTTD) and photonic phase shifting (PPS) have the advantages of ultra-high frequency, true broadband operation, and immunity to

#528338 https://doi.org/10.1364/OE.528338
Journal © 2024 Received 25 Apr 2024; revised 27 May 2024; accepted 27 May 2024; published 12 Jun 2024

Optics EXPRESS

electromagnetic interference [5,9–11]. Especially, the integration of OTTD/PPS in microwave photonic systems has become an effective microwave communication technique with flexible and accurate mode control [3,12].

However, most current reports are either focusing on the bulk-optics-based implementation (large size) or focusing on the integrated OTTD-based methods (limited bandwidth). Moreover, most integrated works only investigate the performance of a single OTTD or PPS element [2,3,7,12,13]. In this paper, we present a novel system-level integrated photonic phased array-based RF-OAM generator-multiplexer on silicon-on-insulator (SOI) platform. The on-chip phased array supports a four-antenna CAA system which can generate/multiplex three OAM modes. The designed RF signal is centralized at 16 GHz due to component/measurement bandwidth limitations. The proposed generator-multiplexer provides the 2-in-1 function of fast mode switching and mode multiplexing. It is composed of a cascaded asymmetric Mach-Zehnder interferometer-based (AMZI-based) interleaved optical filter and a cascaded-heater-based four-channel phased array. By switching the selected pair of wavelengths, the output RF-OAM mode can be fast switched between the fundamental mode, and the ±1 modes. The mode multiplexing can be achieved when loading all three pairs of wavelengths.

2. Principles

A geometric configuration of an N-element CAA for RF-OAM excitation is shown in Fig. 1(a). A pair of phase-locked laser wavelengths with the same frequency spacing as the targeted RF carrier, is fed into an optical phased array. The specially designed phased array will generate different phase shifts between two wavelengths, and each of them is transferred into the RF domain via photodiodes (PDs). The detected signals are used to drive the CAA elements. The N ideal antennas with progressive phases are distributed equidistantly around a circle. In principle, the number of antenna elements (N) determines the largest OAM mode (l_{max}) and it can be expressed as [2]:

$$N>2|l_{max}| \tag{1}$$

A progressive phase shift generated from the phased array is added to different branches of an RF signal before being launched to a CAA, as shown in Fig. 1(a). The step phase shift is given by:

$$\Delta\varphi = \frac{2\pi l}{N} \tag{2}$$

where l is the index of the excited OAM mode. In a four-element CAA system as shown in Fig. 1(b), the allowed OAM modes are l=0 and l=±1, so in total three modes. For the fundamental mode, each antenna should have the same phase (e.g. all 0°). For l=+1 and l=−1, the required step phase shift is 90° and -90°, respectively. Figure 1(b) shows the required phase combinations of fundamental, + 1 and -1 modes: [0°, 0°, 0°, 0°], [0°, 90°, 180°, 270°] and [0°, 270°, 180°, 90°].

Figure 2 presents the operating principles of the proposed fast reconfigurable RF-OAM generator-multiplexer. Two phase-locked optical wavelengths are split into different paths (the shorter wavelength (λ_1) goes into the red path and the longer wavelength (λ_2) goes into the green one.) through an interleaved optical filter. Then the split signal is fed into the two input ports of an optical phased array, separately. For the +1 mode, the phased array will generate four outputs with phase shifts of 0°, 90°, 180°, 270°, respectively, as shown in Fig. 2(a) and Fig. 2(b). These relative phases are transferred into the RF domain after heterodyne beating inside a PD [7]. When choosing λ_3 and λ_4 as presented in Fig. 2(b) OAM: -1 mode case, the shorter and longer wavelengths will exchange output paths of the filter bank (thus the input ports of the phased array are exchanged as well). Without changing the setting of the phased array, the relative electrical phase shifts after beating are reversed to 0°, -90°, -180°, -270°, which correspond to 0°, 270°, 180°, 90° when normalizing to the range between 0° to 360°. Likewise, in the generation of the

Optics EXPRESS

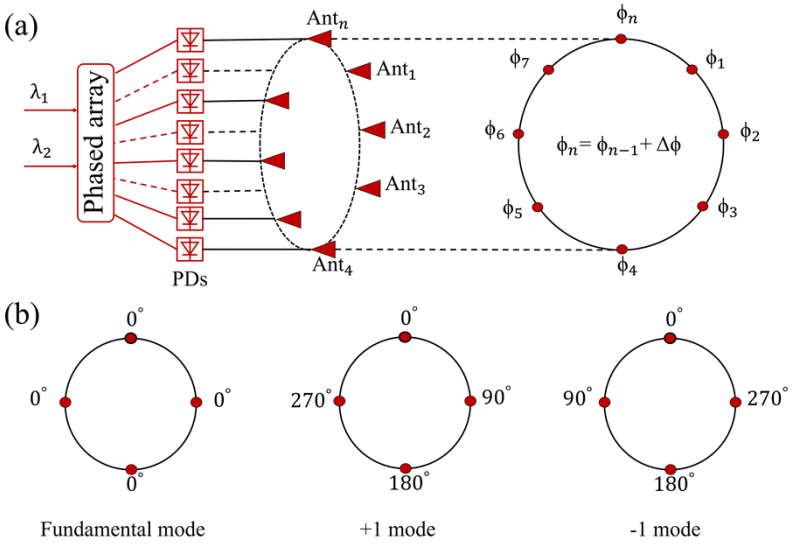

Fig. 1. (a) A typical photonic phased array-driven N-element CAA for RF-OAM generation. (b) The phase distribution of a four-element CAA for 0, and ±1 modes.

fundamental mode, the selection of two wavelengths (λ_5 and λ_6) is orchestrated to ensure that both wavelengths go into one path (e.g. the green path). Then both signals will encounter the same optical phase shift, and thus the relative RF beat phases are 0°, 0°, 0°, 0°. An overview of the mode switching is shown in Fig. 2(c). Fast tunability can be implemented by fast wavelength tuning. The mode multiplexing is achieved by utilizing all three wavelength pairs simultaneously.

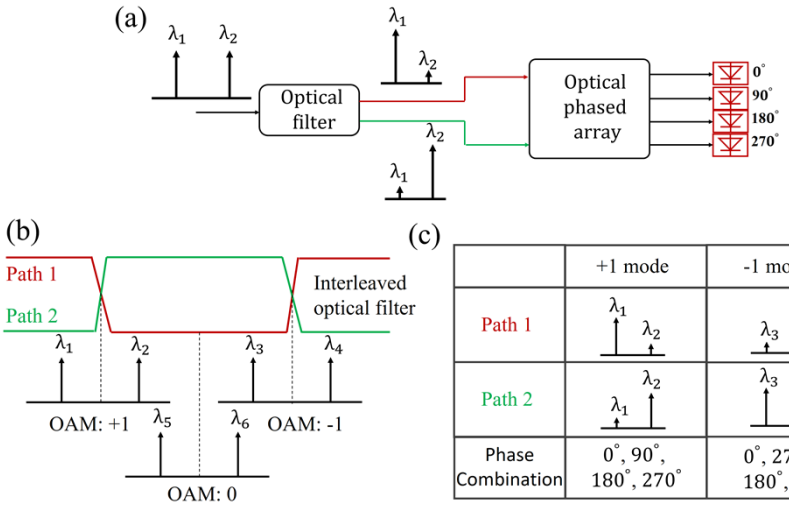

Fig. 2. (a) The proposed RF-OAM generator-multiplexer with +1 mode. (b) The principle of wavelength-tuning-based OAM mode switching; (c) The overview of three OAM mode settings.

Optics EXPRESS

3. Design and simulation

The detailed photonic integrated circuit (PIC) design are presented in Fig. 3. The filter bank is a two-stage-AMZI-based design with a large free spectrum range (FSR-L) at the first stage and a smaller FSR (FSR-S) at the second stage as shown in Fig. 3. The upper output port of the first stage AMZI is connected to the second stage AMZI, directly. The upper output of the second stage AMZI is sent to Path 1, while the other output is first merged with the lower output of the first stage AMZI via a 2-by-1 multimode interferometer (MMI) and is then sent to Path 2. Path 1 is split into four parts using a 1-by-2 MMI-based splitting tree with three tungsten heaters. Here, the heater array is designed as a cascaded layout – one (H1) in the first stage (lower path), two in the second stage (H2 for CH2 and H3 for CH4).

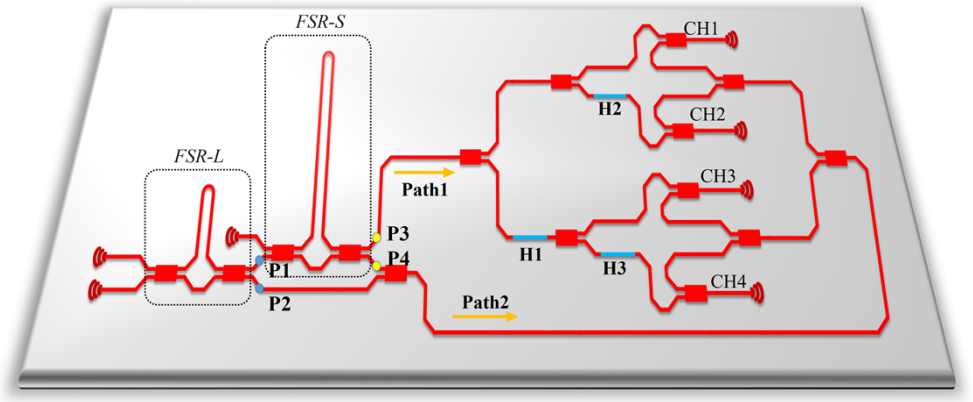

Fig. 3. The schematic diagram of the integrated photonic RF-OAM generator-multiplexer.

In order to better illustrate the principle of the generator-multiplexer, the spectral response of two-stage AMZI is simulated in Lumerical-FDTD/-Interconnect. The length of the delayed waveguide in different AMZI stages are set as 200 μm and 2200 μm. The simulation results is shown in (a) and (b) of Fig. 4. First, two phase-locked optical wavelength λ_1 and λ_2 produced by single sideband (SSB) modulation are fed into the input ports of the devices. The wavelength pairs can be represented as:

$$E_1(t) = A_1\exp(j\omega_c t)\exp(\varphi_1) \tag{3}$$

$$E_2(t) = A_2\exp[j(\omega_c + \omega_{RF})t]\exp(\varphi_2) \tag{4}$$

where A_1, A_2 and φ_1, φ_2 are the amplitudes and phases of the two wavelengths, and ω_c is their carrier frequency, and ω_{RF} is the frequency of the single sideband modulated signal.

For l=±1 mode, the wavelength pair should be aligned to the peak of the upper output port (P1) of the first stage AMZI. This means both two wavelengths are sent to the next stage AMZI. In the second stage AMZI, the two optical tones are aligned and split into two frequency supplementary outputs (P3 and P4) of the AMZI, separately. As presented in Fig. 5(a) and (d), for the +1 mode, λ_1 and λ_2 are selected and finally split to Path 1 (the shorter wavelength) and Path 2 (the longer wavelength), individually. The desired RF carrier frequency equals to a half FSR of the second stage AMZI. When λ_1 and λ_2 are recombined at the final output, the optical signal can be expressed as:

$$\begin{aligned} E(t) = {} & A_1\exp(j\omega_c t)\exp(\varphi_1 + \psi_{AMZI1} + \psi_{AMZI2} + \theta_{path1,i}) + A_2\exp[j(\omega_c + \omega_{RF})t]\exp(\varphi_2 \\ & + \psi_{AMZI1} + \psi_{AMZI2} + \theta_{path2,i}) \end{aligned} \tag{5}$$

where ψ_{AMZI1} and ψ_{AMZI2} represents the phase shift caused by the cascaded AMZI, the i=1,2,3,4, represents the i output channel in the phased array, $\theta_{path1,i}$ is the phase shift generated by heater

Optics EXPRESS

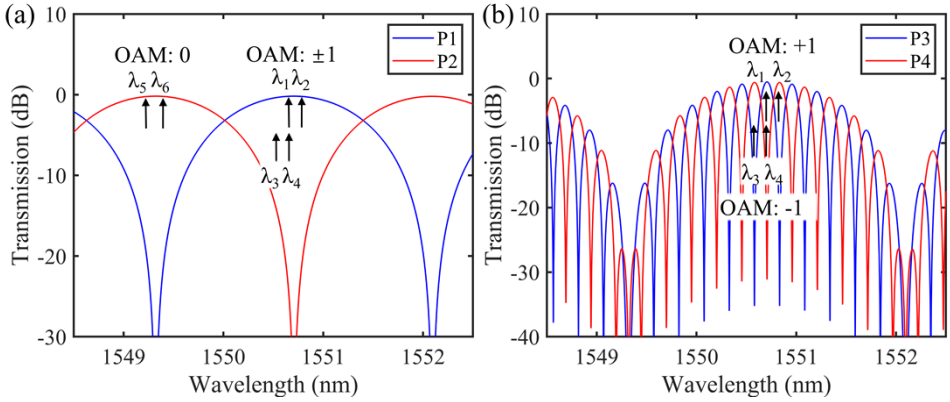

Fig. 4. (a) The spectral response of the first stage AMZI simulated by Interconnect. (b) The spectral response of the second stage AMZI simulated by Interconnect.

array in path1 to the i output channel, resulting in the phase offset of [0°, 90°, 180°, 270°], $\theta_{\text{path2},i}$ is the phase shift in path 2 to the i output channel, resulting in a phase shift of [0°, 0°, 0°, 0°]. The combined light signal is converted into a radio frequency signal after the photodetector beats:

$$i_{RF} \propto RA_1A_2\cos[\omega_{RF}t + (\varphi_1 - \varphi_2) + \theta_{RF,i}] \tag{6}$$

where R is the responsivity of the PD, $\theta_{RF,i} = \theta_{\text{path1},i} - \theta_{\text{path2},i}$, represents the phase shift of the radio frequency signal of the i channel. So the phase difference between the two adjacent channels is +90°.

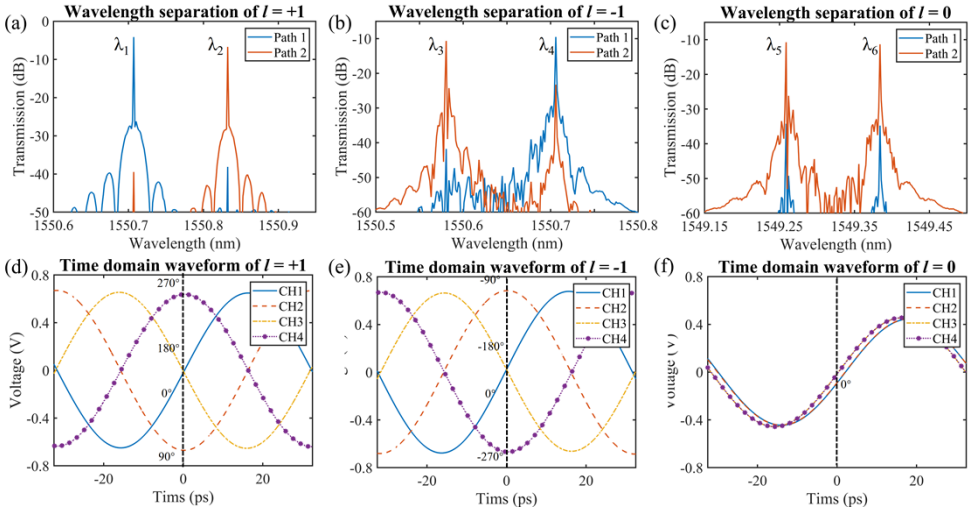

Fig. 5. Interconnect simulation results: (a) - (b) Wavelength separation in three OAM modes. (d) - (f) Time domain waveforms of four output channels in three OAM modes.

Then switching from the +1 mode to -1 mode can be achieved by shifting the carrier with a half FSR-S (λ_3 and λ_4, $\lambda_3 = \lambda_2$) to exchange the wavelength-path mapping order (Path 2 -\gt the shorter wavelength, and Path 1 -\gt the longer wavelength). In this case, $\theta_{RF,i} = \theta_{\text{path2},i} - \theta_{\text{path1},i}$, so the phase difference between the two adjacent channels is -90°, as shown in Fig. 5(b) and (e). When setting to fundamental mode, the wavelength pair (use λ_5 and λ_6) is aligned to the lower

Optics EXPRESS

output port (P2) of the first stage AMZI (red curve in Fig. 4(a)). As can be seen in Fig. 5(c) and (f), both wavelengths will bypass the second stage AMZI and go into the Path 2 directly, and $\theta_{RF,i} = \theta_{\text{path2},i} - \theta_{\text{path2},i}$, so that the four output channels have the same phase.

4. Experiments and results

The designed PIC is fabricated in IMEC's SOI platform and shown in the inset of Fig. 6(b). The PIC is wire bonded and driven by our designed system including voltage/current sources and control algorithms. The measurement experiments schematic block diagram of the generator-multiplexer are presented in Fig. 6(a). A tunable external cavity laser (ECL, Pure Photonics PPCL600) with a power of +13 dBm is first fed into a Mach-Zehnder modulator (MZM, Fujitsu, FTM7938EZ), which is driven by an amplified 16-GHz RF signal via an electrical amplifier (EA, Centellax, OA4MVM3) from a vector network analyzer (VNA, Rohde & Schwarz ZNB40). The modulated optical signal (+2 dBm) will have three frequency tones (one carrier and two 16-GHz sidebands), and then is tuned to transverse electromagnetic (TE) mode by an optical polarization controller (PC) before going into the PIC. The signal is sent to the PIC input grating coupler via a cleaved fiber. The measured coupling loss from fiber to PIC is ~3.05 dB/coupler. In principle, four on-chip PDs could be placed for optical-electrical-conversion. However, since the MPW is a passive MPW without active components, four grating couplers are utilized as the final array-outputs. An off-chip PD is used to convert the signal into the electrical domain and feed it back to the VNA for phase/intensity measurements. By moving the output cleaved fiber to different output grating couplers, the relative phase shifting curves of four channels can be obtained. The direct output signal of the PIC has three wavelength tones, of which one sideband is then eliminated by an optical tunable filter (OTF, Santec OTF-350) to create the two-wavelength input signal for the PD. To compensate the loss from modulation/PIC propagation/PIC coupling, an erbium-doped fiber amplifier (EDFA, Amonics, AEDFA-IL-23-B-FA) is introduced to boost the signal before the optical filter. Finally, the carrier together with a single upper sideband is tuned to -7 dBm by changing the EDFA gain and is sent to the PD/VNA. The experimental system is shown in Fig. 6(b). In order to ensure precise alignment of the wavelength, temperature is stabilized at 25°C by a thermoelectric heater/cooler (TEC) with a thermistor packaged with the PIC, as variations in ambient temperature can lead to spectral drift in the filter.

In order to test different OAM modes, it is essential to select a correct wavelength pair as shown in Fig. 7(a) and (b). Initially, two independent AMZIs structures identical to the two-stage AMZIs of Fig. 3 are tested separately, with their spectral responses presented in Fig. 7(a) and (b) individually. The FSR-L of the first stage AMZI and the FSR-S of the second stage AMZI are measured to be 2.82 nm and 0.25 nm respectively. The responses of the in-system AMZI filters may shift left or right, so more precise wavelength alignment can be assessed by monitoring interference spectrum at the output port, as any misalignment will cause optical power leakage into an alternate path. Only when precisely aligned can the wavelength pair be well separated, with the output optical power remaining essentially stable even if there are changes in optical phase.

To investigate the efficiency of phase tuning in a single heater, different electrical powers are applied to H3 (in CH4) to examine their impact on RF phase shifting. The power varies from 0 mW to 60 mW with a stepwise increase of 5 mW, and the relative phases shifting to 0 mW over a sweeping range of 1 GHz RF are shown in Fig. 8(a). Figure 8(b) depicts the relationship between the relative phase of the central frequency of 16 GHz and the applied heating power. As illustrated in the figure, it is evident that the heating power is already sufficient to generate a 360-degree phase shift, and their relationship appears to be approximately linear.

The alignment of laser wavelength pairs in three modes are illustrated in Fig. 9. Initially, the laser carrier wavelength is adjusted to 1550.91 nm to achieve the $l = +1$ mode. The carrier and sideband are then separated in Path 1 and Path 2, respectively, by the cascaded AMZI filter. In

Optics EXPRESS

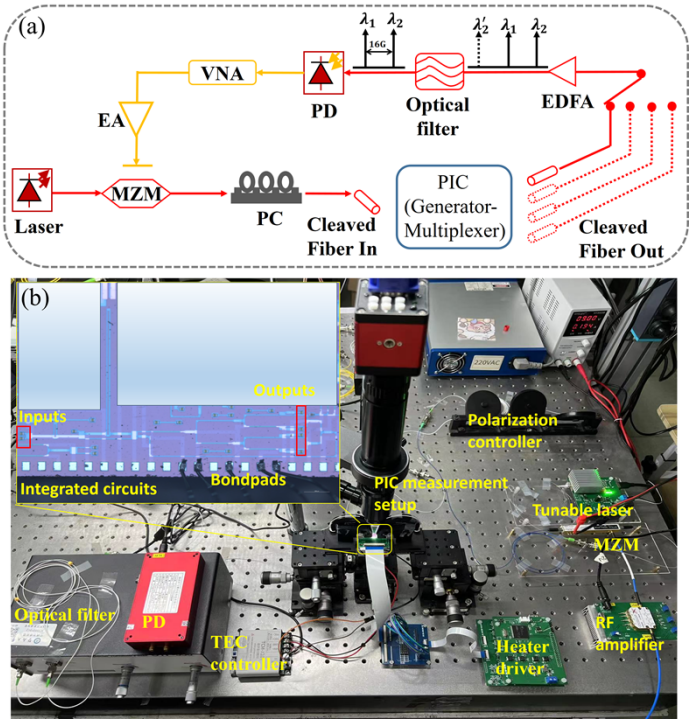

Fig. 6. (a) The schematic block diagram of measurement system. (b) The experimental setup.

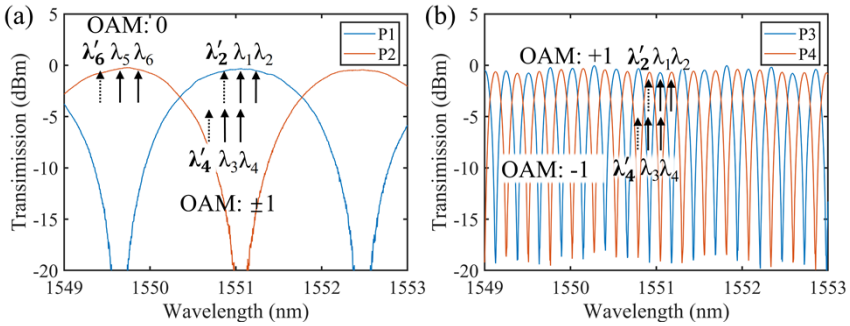

Fig. 7. (a) The reference spectral response of the AMZI with a larger FSR from a test structure. (b) The reference spectral response of the AMZI with a small FSR from a test structure.

Path 1, different relative phase shifts [0°, 90°, 180°, 270°] are generated in the four channels using a cascaded heater array with power inputs of 22 mW for heaters H1 and H2, and 13 mW for heater H3. As depicted in Fig. 10(a) to (f), a VNA is used to evaluate the phase and intensity response of the four output channels by sweeping a sinusoidal signal range from 15.5 GHz to 16.5 GHz with CH1's phase calibrated to zero. The measured relative phase shift from CH2 to CH4 is found to be within a maximum standard deviation of 2.97° with a maximum relative power shift of 0.5 dB. Then the laser wavelength is switched to approximately 1550.78 nm to implement the $l = -1$ mode, and the carrier and sideband will exchange output ports of the second stage AMZI. Due to filter-related residual optical interference, slight adjustments are made to the powers

Optics EXPRESS

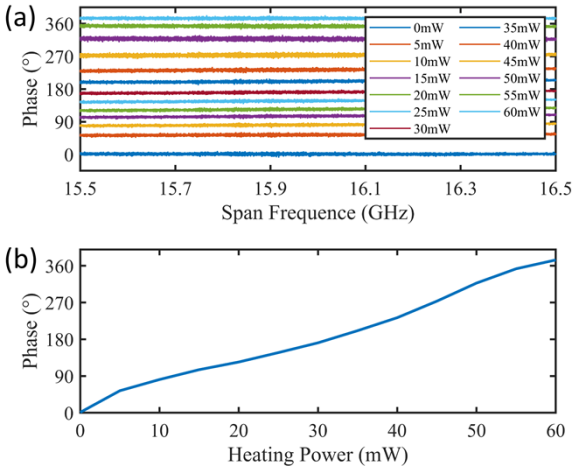

Fig. 8. (a) The phase shifting of CH4 as the power of heater H3 is increased from 0 mW to 60 mW during a 1-GHz sweeping range. (b) The relationship between the relative phase of the central frequency of 16 GHz and the applied heating power.

of the heaters, which are set at 21 mW, 26.5 mW, and 10 mW for fine phase correction. The phase difference of adjacent channels from CH1 to CH4 is set at -90°. The maximum standard deviation of the measured phase error is 1.80° and the maximum relative power shift is 1.1 dB. In terms of the fundamental mode, the laser wavelength is tuned to 1549.33 nm, with whose sideband both wavelengths are feed into the non-phase-shifting path. As shown in Fig. 10(d), all four channels exhibit nearly identical phase and intensity responses. In the proposed cascade layout, H1 introduces a 180° phase shift that is shared by CH3 and CH4, thereby enhancing the energy efficiency of heaters.

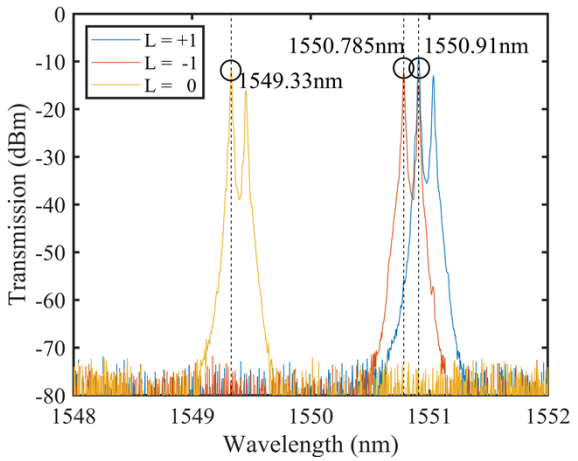

Fig. 9. The spectrum of the single sideband modulated signal in three OAM modes.

Optics EXPRESS

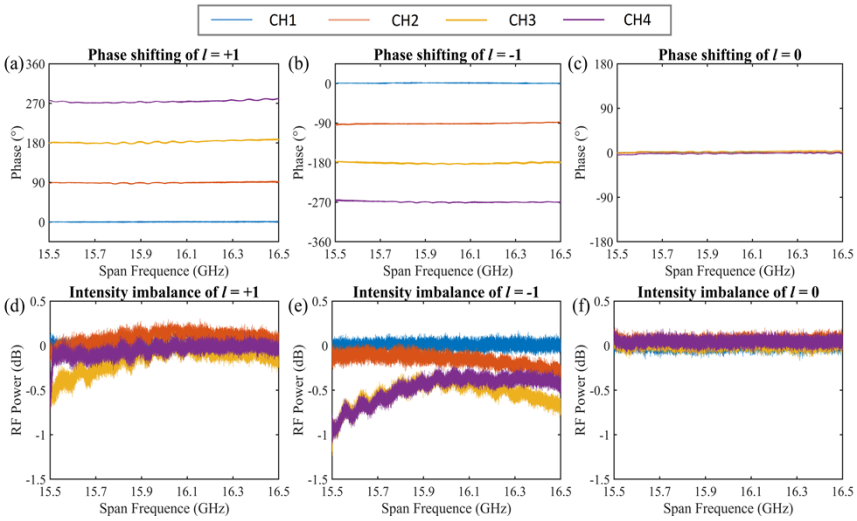

Fig. 10. (a) - (c) The measured relative phase response in three OAM modes. (d) - (f) The measured intensity response in three OAM modes.

5. Conclusion

In this paper, a novel integrated photonic RF-OAM generator-multiplexer for a four-antenna CAA system has been proposed and experimentally demonstrated. The system consists of a cascaded AMZI with different FSRs and a cascaded heater array and supports three RF-OAM modes at 16 GHz with a 1-GHz RF bandwidth. Fast mode switching can be implemented by using wavelength switching, and mode multiplexing can be achieved by loading all 6 wavelengths in principle. It is important to note that the RF frequency/bandwidth can be extended by designing a sharper transition zone, flat-top, and broadband interleaved filter [13]. In principle, an OAM mode change can be accomplished by only wavelength tuning. Here a slight heating adjustment is used to do the fine phase correction due to the imperfect interleaved filter bandwidth/crosstalk. This may be resolved by a better filter design. The heating efficiency can be further improved with a 4-mW-per-pi phase shifter [14]. By increasing the number of interlaced filters and the input path of the phased array, a larger scale CAA (e.g. 8-membered CAA) can be supported and higher-order OAM modes can be generated.

Funding. National Natural Science Foundation of China (62175092); Natural Science Foundation of Guangdong Province (2023A1515011155); Guangzhou Basic and Applied Basic Research Foundation (202201010088).

Acknowledgment. The authors would like to thank IMEC MPW Run for the PIC fabrication.

Disclosures. The authors declare no conflicts of interest

Data availability. Data underlying the results presented in this paper are not publicly available at this time but may be obtained from the authors upon reasonable request.

References

1. A. E. Willner, Y. Ren, G. Xie, *et al.*, "Recent advances in high-capacity free-space optical and radio-frequency communications using orbital angular momentum multiplexing," Phil. Trans. R. Soc. A. **375**(2087), 20150439 (2017).
2. X. Gao, S. Huang, Y. Song, *et al.*, "Generating the orbital angular momentum of radio frequency signals using optical-true-time-delay unit based on optical spectrum processor," Opt. Lett. **39**(9), 2652 (2014).
3. M. Zhao, S. Xia, X. Zhang, *et al.*, "Photonic Radio Frequency Orbital Angular Momentum Generation and Beam Steering," J. Lightwave Technol. **41**(7), 2107–2115 (2023).
4. S. M. Mohammadi, L. K. S. Daldorff, J. E. S. Bergman, *et al.*, "Orbital angular momentum in radio—a system study," IEEE Trans. Antennas Propag. **58**(2), 565–572 (2010).

Optics EXPRESS

5. X. Gao, S. Huang, Y. Wei, *et al.*, "An orbital angular momentum radio communication system optimized by intensity controlled masks effectively: Theoretical design and experimental verification," Appl. Phys. Lett. **105**(24), 241109 (2014).
6. S. Yu, L. Li, G. Shi, *et al.*, "Design, fabrication, and measurement of reflective metasurface for orbital angular momentum vortex wave in radio frequency domain," Appl. Phys. Lett. **108**(12), 121903 (2016).
7. J. Capmany and D. Novak, "Microwave photonics combines two worlds," Nat. Photonics **1**(6), 319–330 (2007).
8. J. Yao, "Microwave Photonics," J. Lightwave Technol. **27**(3), 314–335 (2009).
9. M. Xie, M. Zhao, M. Lei, *et al.*, "Anti-dispersion phase-tunable microwave mixer based on a dual-drive dual-parallel Mach-Zehnder modulator," Opt. Express **26**(1), 454 (2018).
10. J. Huang, Z. Cao, X. Zhao, *et al.*, "Optical generation/detection of broadband microwave orbital angular momentum modes," J. Lightwave Technol. **38**(6), 1202–1209 (2020).
11. Y. Yan, G. Xie, M. P. J. Lavery, *et al.*, "High-capacity millimetre-wave communications with orbital angular momentum multiplexing," Nat. Commun. **5**(1), 4876 (2014).
12. M. Zhao, X. Zhang, N.-C. Tran, *et al.*, "Integrated tunable phase shifter based on energy-conserved phase amplification and its application for RF-OAM generation," IEEE J. Select. Topics Quantum Electron. **1**, 1 (2020).
13. J. S. Fandiño, P. Muñoz, D. Doménech, *et al.*, "A monolithic integrated photonic microwave filter," Nat. Photonics **11**(2), 124–129 (2017).
14. R.-L. Chao, Z. Ahmad, J. Chen, *et al.*, "BJT-type optical phase shifter with small power consumption and fast response time on a silicon photonics foundry platform," IEEE J. Select. Topics Quantum Electron. **26**(2), 1–7 (2020).

146.102.254.11 2025-10-27 05:05:4